

Geometrical design for pure current-driven domain wall nucleation and shifting EP

Cite as: Appl. Phys. Lett. **121**, 102403 (2022); <https://doi.org/10.1063/5.0106689>

Submitted: 29 June 2022 • Accepted: 16 August 2022 • Published Online: 07 September 2022

 D. Osuna Ruiz,  O. Alejos,  V. Raposo, et al.

COLLECTIONS

 This paper was selected as an Editor's Pick



View Online

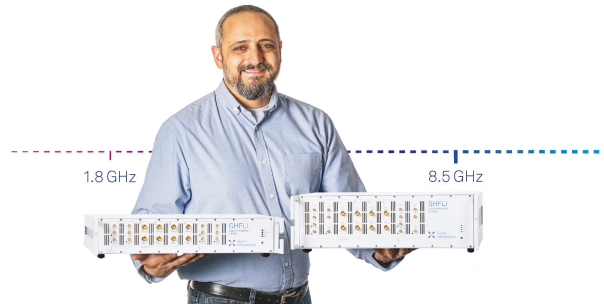


Export Citation




CrossMark





Trailblazers. New

Meet the Lock-in Amplifiers that measure microwaves.

 Zurich Instruments [Find out more](#)

Geometrical design for pure current-driven domain wall nucleation and shifting

Cite as: Appl. Phys. Lett. **121**, 102403 (2022); doi: [10.1063/5.0106689](https://doi.org/10.1063/5.0106689)

Submitted: 29 June 2022 · Accepted: 16 August 2022 ·

Published Online: 7 September 2022



View Online



Export Citation



CrossMark

D. Osuna Ruiz,^{1,a)}  O. Alejos,²  V. Raposo,¹  and E. Martínez¹ 

AFFILIATIONS

¹Department of Applied Physics, University of Salamanca, Salamanca 37008, Spain

²Department of Electricity and Electronics, University of Valladolid, Valladolid, Spain

^{a)}Author to whom correspondence should be addressed: osunaruiz.david@usal.es

ABSTRACT

Nucleation of domain walls by current-driving a single domain wall, confined to the junction area of two symmetrical strips, is investigated using systematic micromagnetic simulations. Secondary domain walls (equivalently, bits encoded in domains) are simultaneously nucleated and driven by alternatively applying current pulses between two terminals in the structure. Simulations show that nanosecond-duration current pulses nucleate and drive series of robust up/down domains even under realistic conditions. These results demonstrate a technique for sequentially nucleating and shifting domain walls without using attached external “bit lines,” fields, or modifying the ferromagnetic strip.

Published under an exclusive license by AIP Publishing. <https://doi.org/10.1063/5.0106689>

A magnetic domain wall (DW) consists of a transition region of magnetization that separates two magnetic domains. These magnetic configurations are interesting, not only for their fundamental physics but also for technological applications.^{1,2} In particular, DW dynamics have attracted special attention in ultrathin ferromagnetic (FM) films that show high perpendicular magnetic anisotropy (PMA), sandwiched in a multilayered structure between a Heavy Metal (HM) layer and typically an oxide (Ox) layer.^{3–7} The interfacial Dzyalozhinski–Moriya Interaction (iDMI) present in those structures promotes homochiral Neel DWs separating “up” or “down” domains.⁸ These domains can be potentially exploited as information bits. An electrical current in the HM layer is used to drive the chiral Neel DWs along the FM strip via spin–orbit torques (SOTs).^{4,7} Also, they can be compactly stored and driven along magnetic tracks.²

For data-recording applications, DW-based devices must be efficient in three typical stages of operation, namely, writing, moving, and reading bits (domains). The second stage is typically implemented by using SOTs to shift DWs and the third one by reading the out-of-plane magnetization using a magnetic tunnel junction (MTJ). However, prior to all the above, domain and DW nucleation (or writing bits) are necessary as a first step. An Oersted magnetic field from an attached current bit line is typically used, which locally reverses magnetization in the strip. However, the Oersted field that nucleates a new DW can also annihilate already shifted DWs.⁹ Note that due to the long-range dependence of the Oersted field, a standard bit-line architecture is not useful to nucleate subsequent DWs without perturbing the

information already coded in the up or down domain between them (see details in Ref. 9). To solve this issue, solutions based on modifying the strip geometry,¹⁰ adding more voltage terminals,^{11,12} or using a double bit line configuration have been proposed.⁹ However, these solutions still require external attachments and a more intricate multi-layer design.

Other proposals for nucleation of chiral Neel DWs in PMA strips rely on electric fields or ion beam irradiation, which induces local changes in the local magnetic anisotropy.^{13,14} In this way, nucleation and injection of chiral DWs have also been demonstrated by modifying the magnetic properties of the strip. For example, Dao *et al.*¹⁵ nucleated and injected chiral DWs by a tailored “in/out-of-plane” magnetization boundary, strategically placed in the strip. For this, a precise local control on magnetic anisotropy is still required. Also in Ref. 15, domains of $\sim 1 \mu\text{m}$ wide were obtained by injecting current pulses in the presence of external in-plane magnetic fields. Simpler mechanisms for nucleation of packed chiral DWs, without manipulating the magnetic anisotropy nor using magnetic fields, remain elusive,¹⁶ which is a key first step for developing efficient DW-based recording devices.

Here, we explore an approach based on a single current-driven DW, confined to the junction area of two symmetrical strips, that works as a DW nucleator. The subsequent domain series is coherent with the input pulsed current without the need of external magnetic fields or attachments. In what follows, we first describe the micromagnetic model used for our simulations. After that, we present and

discuss the results from ideal and realistic scenarios, typically found in experiments. Finally, the main conclusions are summarized.

Figure 1(a) shows a schematic of the simulated HM/FM/Ox strip geometry, with width $w = 96$ nm, thickness $t_{FM} = 0.6$ nm, and aperture half-angle $\theta = 45^\circ$. Its initial magnetization state at equilibrium is also shown. The geometry consists of three combined strips, two of them are symmetrical with respect the central, longitudinal strip. For convenience, herein we refer to them as the “Top-Left strip” (TL), “Bottom-Left strip” (BL), and “Register strip” (R), as depicted in Fig. 1(a). Typical Pt/Co/Ox parameters were adopted:^{4–6,18} exchange constant $A_{ex} = 1.6 \times 10^{-11}$ J m⁻¹, saturation magnetization $M_S = 0.8 \times 10^6$ A m⁻¹, anisotropy constant $K_U = 0.8 \times 10^6$ J m⁻³, and DMI parameter $D = -1.2 \times 10^{-3}$ J m⁻².¹⁵ HM layer lays below the FM layer, with the same layout. The up and down domains at the TL and BL strips act as “bit reservoirs.” A detection area (orange shaded area) at ~ 300 nm from the junction area represents an MTJ for reading the local out-of-plane magnetization (m_z). A magnetic configuration with PMA is represented, where the DW is a chiral Neel type wall.⁸ A more detailed discussion on the nucleation of the initial DW, required by standard techniques, can be found in the [supplementary material](#).

Starting from the initial state shown in Fig. 1(a), current pulses (J_1 or J_2) are injected by applying voltage pulses between terminals [blue lines in Fig. 1(a)] at the TL or BL strip and the R strip (i.e., V_1 or V_2 , depending on the switch position). Then, the magnetization

dynamics is numerically investigated by solving the following LLG equation:

$$\frac{d\vec{m}(t)}{dt} = -\gamma_0 \vec{m}(t) \times \vec{H}_{eff} + \alpha \vec{m} \times \frac{d\vec{m}(t)}{dt} + \vec{\tau}_{SOT}, \quad (1)$$

where $\vec{\tau}_{SOT}$ accounts for the SOT due to the Spin Hall Effect (SHE), and $\vec{\tau}_{SOT} = -\gamma_0 H_{SL}^0 \vec{m} \times (\vec{m} \times \vec{\sigma})$. $\vec{\sigma}$ is the spin current polarization that satisfies $\vec{\sigma} = \vec{u}_z \times \vec{u}_J$, where \vec{u}_z is the unit vector direction along the spin current \vec{J}_S and \vec{u}_J is that of the applied current \vec{J} . $H_{SL}^0 = \frac{\hbar \theta_{SH} J}{2|e|\mu_B M_S t_{FM}}$ defines the Slonczewski-like-SOT magnitude, which is proportional to J . Micromagnetic simulations were performed using Mumax3,¹⁹ considering SHE angle $\theta_{SH} = 0.12$ and Gilbert damping constant $\alpha = 0.1$.¹⁸ Cell sizes along x , y , and z were fixed to 1, 1, and 0.6 nm, respectively. A more detailed description of the micromagnetic model can be found elsewhere.²⁰ Figure 1(b) shows streamlines for an inhomogeneous $\vec{J} = \vec{J}(\vec{r}) = J(x, y)\vec{u}_J$ as well as for $\vec{\sigma}$ when $V_2 = 1$ and $V_1 = 0$ V are applied, obtained from COMSOLTM,¹⁷ for $\theta = 45^\circ$.

Sequential nucleation of domains in the R (register) strip can be characterized as phase diagrams for each combination of J and pulse duration d . Micromagnetic results reveal that two different “states” can be obtained. These states will determine the success of nucleating domains in sequence. Figures 2(a) and 2(b) show two exemplary cases, obtained after applying the pulse sequences depicted in the top panels, for $J = 2.5$ TA/m² and the indicated d and τ (time between consecutive pulses) in each case. Their related output signals (m_z) at the reading position are shown in the middle panels. Bottom panels in Figs. 2(a) and 2(b) show timestamps of m_z for the respective d and τ in each case. For $d = 0.2$ ns [Fig. 2(a)], the DW does not reach the opposite edge of the strip and relaxes into a new equilibrium position in the BL strip during τ . For $d = 0.5$ ns [Fig. 2(b)], the DW reaches the edge within the duration of each pulse, before splitting and nucleating a DW in the R strip. Only the latter situation leads to an operational DW nucleating performance, where the nucleated domains are correlated with the input sequence of J . For simplicity, we call these two possible outcomes: “Un-triggered” state [Fig. 2(a)] and “Nucleator” state [Fig. 2(b)].

This purely geometrical method can generate any domain sequence, as the same process shown in Fig. 2(b) can be replicated in next pulse iterations. The working principle is as follows: a voltage pulse V_2 (V_1) is applied between terminals of the BL (TL) and R strips, generating a both “nucleating” and “driving” current J_2 (J_1). The generated current drives a DW, previously nucleated at the BL or TL strip (BL in Fig. 2), into the R strip. The nucleation of such first DW is performed only once by standard ways, for example by injecting a current along a bit line (see the additional simulations and related discussion in the [supplementary material](#)). Driven by J (J_2 in Fig. 2), the DW will eventually stop before reaching the start of the opposite symmetric strip, since current is not flowing there [see Figs. 2(a) and 2(b)]. The nucleation of new DWs into the R strip is possible after the driven DW splits at the opposite edge of the structure, depending on the applied pulse intensity J (J_1 or J_2) and duration d . If J is greater than a critical current (J_C), two new DWs are obtained: one that is simultaneously formed and driven by the same applied current along the R strip, and another one that “regenerates” the confined DW but now of opposite type [“down-up” in the sixth timestamp in Fig. 2(b)] and placed at the other symmetric strip. Nucleated DWs in the R strip will

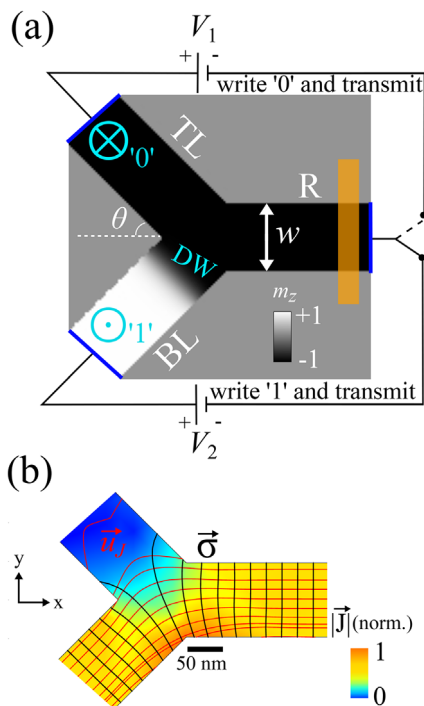


FIG. 1. (a) Scheme showing the symmetric strip structure modeled in simulations. The PMA configuration is shown by the up/down domains and the separating DW. The input current pulses, alternated between the symmetric arms, are represented by a switch and a potential difference between terminals. (b) Streamlines of \vec{J} (red) and $\vec{\sigma}$ (black) are shown, obtained from COMSOLTM when V_2 is applied. Color scale represents the (normalized) magnitude of the resulting inhomogeneous J .

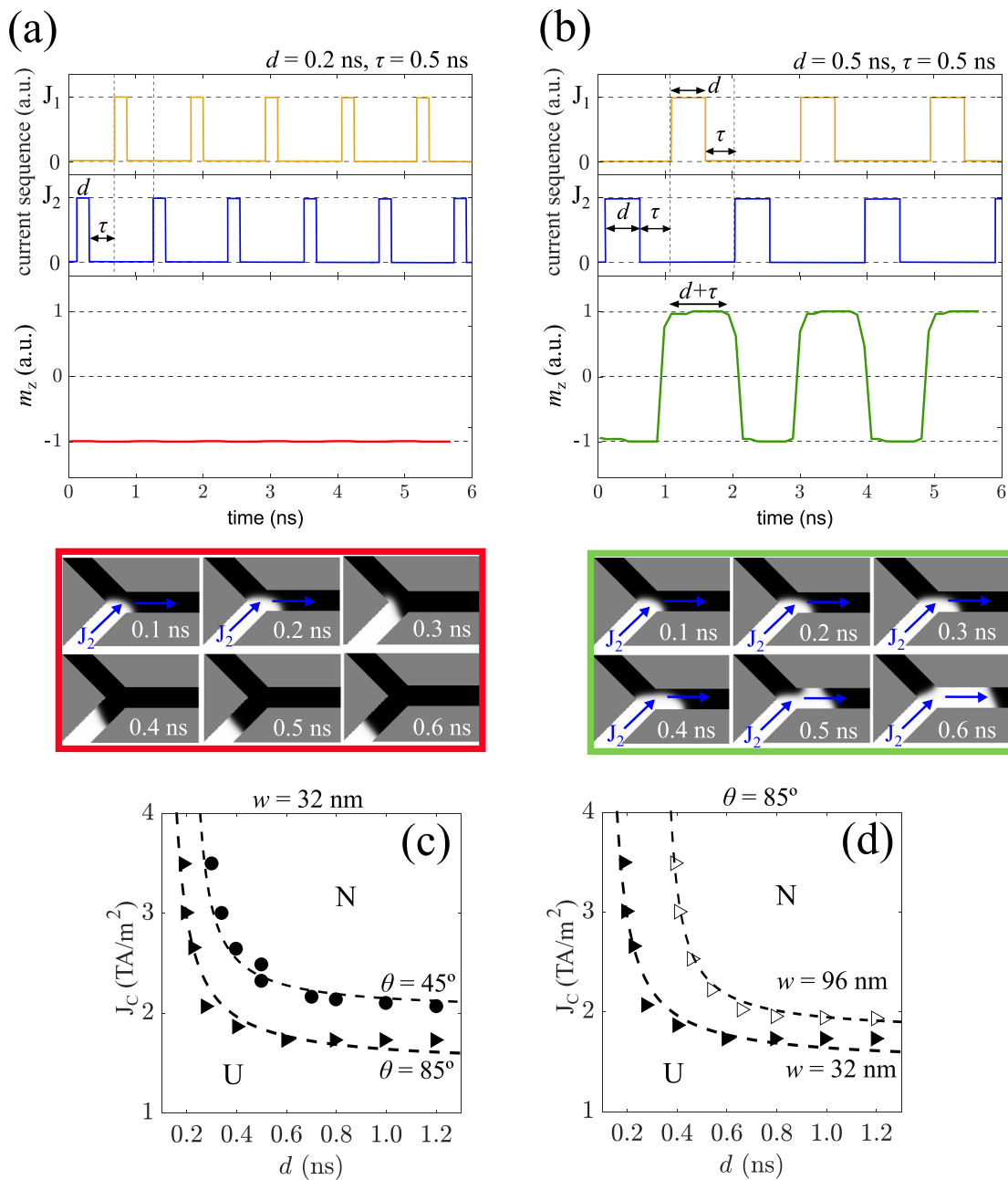


FIG. 2. (a) and (b) (Top panels) Current pulse sequences for two exemplary cases and (middle panels) their associated readout signal (i.e., normalized m_z at the “detector position” or orange area), as a response to the pulses. (Bottom panels) Snapshots of the instantaneous DW position for a single J_2 pulse excitation showing the out-of-plane magnetization, m_z , for the two states found in simulations. (c) Summarized full micromagnetic results for J_C vs d for $\theta = 45^\circ$ (circles) and $\theta = 85^\circ$ (triangles). Full symbols indicate the $J_C - d$ “boundary” beyond which “Nucleation” state was achieved. Dashed curves are for guiding the eye. (d) Summarized results for two different widths, 96 and 32 nm, and $\theta = 85^\circ$.

be driven independently of activating either J_1 or J_2 . Thus, by alternatively applying current pulses between the TL or BL strip and the R strip, up or down domains can be simultaneously nucleated and driven.

Then, regarding practical purposes, one question arises: how could we optimize information (domain) density in the R strip? To get

further insight, Fig. 2(c) shows a summarized state/phase diagram for each combination of J_C and d explored in simulations for $\theta = 45^\circ$ (circles) and $\theta = 85^\circ$ (triangles) and $w = 32$ nm. Similar results were also obtained for other $\theta < 90^\circ$ and also for $w = 96$ or $w = 10$ nm. Figure 2(d) shows similar qualitative results for $w = 96$ nm. A more

detailed analysis on the influence of w is provided in the [supplementary material](#). As expected, the critical current above which DW nucleation is achieved, reduces with increasing d . Also, the $J_C(d)$ curve is displaced downward with reducing w and/or increasing θ . As discussed in the [supplementary material](#), the efficiency of the SOT promoting the DW nucleation is enhanced as θ increases for a given w . In addition, one may expect that a higher domain density in the R strip can be obtained for high (small) J and small (high) d , as the DW will be moving faster for a fixed time (or for longer time for a fixed velocity). However, at the cases where J or/and d are very high, undesirable effects arise due to spontaneous domain nucleation along the strip,²¹ resulting in a faulty sequence, as observed in our simulations

(not shown). Also, smaller J_C require larger d for DW nucleation, which leads to wider domains and therefore reduces the information density. Using wider strips would further allow to reduce J_C , but at the expense of increasing d . For all the above, an optimal density of domains is expected when both J_C and d are minimized, and by increasing θ and/or reducing w .

So far, we explored the performance of the proposed method under ideal conditions, i.e., no thermal fluctuations ($T=0$ K), grain structure, or rounded geometrical features. To get a better insight, we explore the performance of a more realistic strip accounting for thermal fluctuations at room temperature ($T=300$ K), grains and rounded kinks, with $\theta=85^\circ$. Following

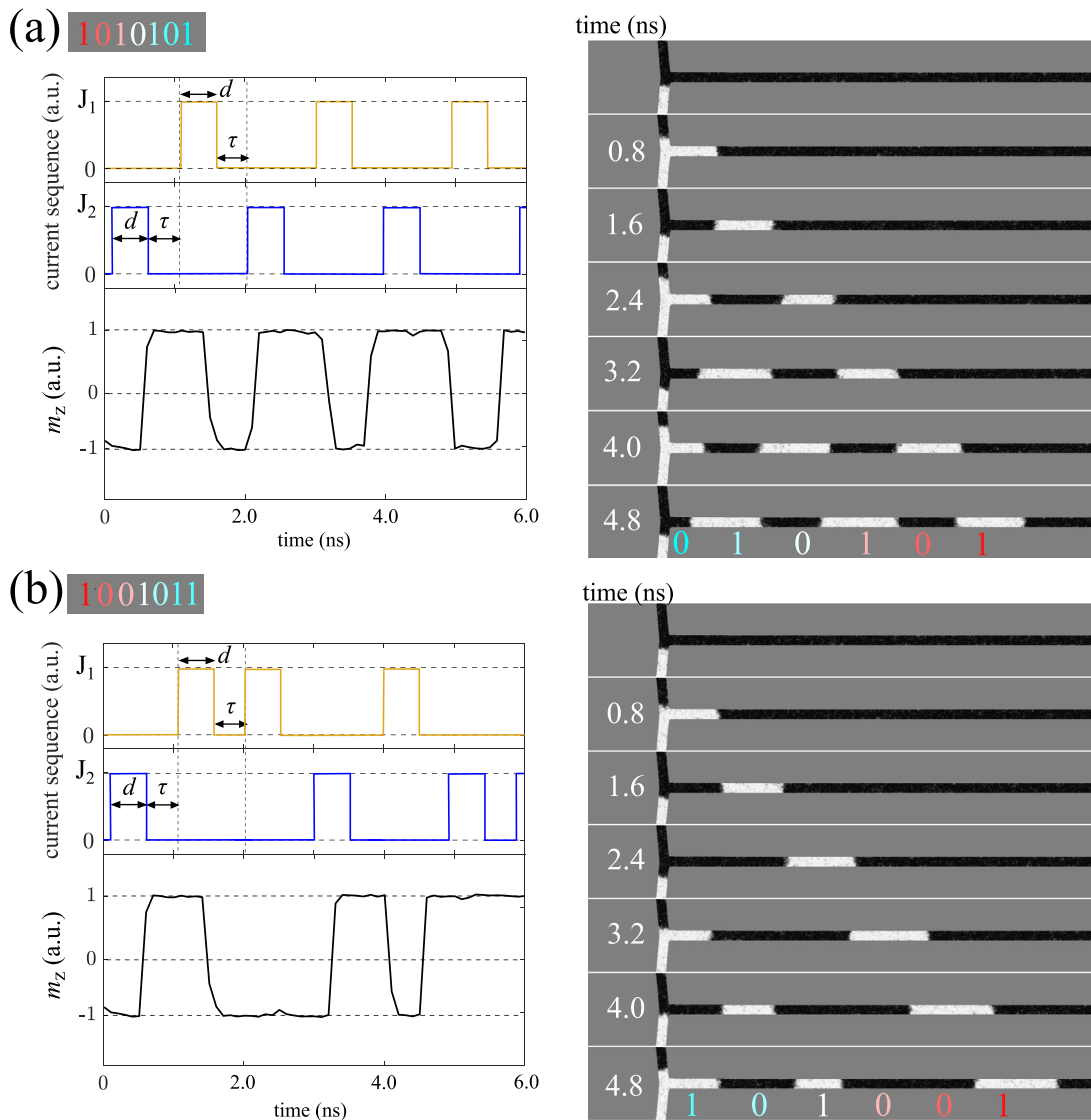


FIG. 3. (a) Current pulse sequence (top left panel) and normalized m_z at the detector area (bottom left panel) for $J=2.0$ TA/m² and $d = \tau = 0.4$ ns for the bit sequence “1010101” ($J_1 \sim '0'$ and $J_2 \sim '1'$). Timestamps of m_z are shown in the right panels (normalized, black is -1 and white is $+1$) under realistic conditions. (b) Equivalent results for the bit sequence “1001011.”

from previous studies,²⁰ the grains are modeled as a random deviation of maximum 10% of K_U from its original direction (\vec{u}_z) in irregular sized regions of 3 nm radius on average. Rounded kinks of radius 30 nm are considered.

Two bit input sequences “1-0-1-0-1-0-1” and “1-0-0-1-0-1-1,” encoded into m_z by the pulse sequences $J_2 \rightarrow J_1 \rightarrow J_2 \rightarrow J_1 \rightarrow J_2 \rightarrow J_1 \rightarrow J_2$ and $J_2 \rightarrow J_1 \rightarrow J_1 \rightarrow J_2 \rightarrow J_1 \rightarrow J_2 \rightarrow J_2$ [shown in the top graphs in Figs. 3(a) and 3(b)], respectively, are simulated for $J = 2.0 \text{ TA/m}^2$ and $d = \tau = 0.4 \text{ ns}$ under realistic conditions for a 32 nm wide strip. Figures 3(a) and 3(b) shows m_z as a function of time (bottom graphs) and timestamps of the nucleated “domain sequence” for both bit sequences. They reveal that the input current-pulse signals are effectively replicated along the R strip and correctly detected through m_z under realistic conditions. Therefore, nucleation of domain sequences coherent with the input pulses is demonstrated as proof-of-concept. Additional simulations were also performed taking into account the influence of a Field-Like (FL-SOT) torque comparable in magnitude to the SL-SOT. The results, presented in the [supplementary material](#), indicate that the working principle of our proposed method remains valid in the presence of FL-SOT. Moreover, the role of the non-uniform Joule heating has been also analyzed as described in the [supplementary material](#). Such results point out that the proposed nucleation and shifting method still remains valid.

To conclude, we have devised a method to nucleate DWs with just three terminals, purely by current methods without requiring multilayer attachments, external magnetic fields, or actively modifying the magnetic properties of the strip. A symmetric three-strip structure with a confined chiral Neel DW in the center is used as an optimal DW nucleator as a function of J and d . The design here proposed is simpler than those found in literature that are based on similar principles^{11,12} and typically require multiple terminals for nucleating and driving DWs not concurrently¹² or locally attached metallic wires for injecting currents. Compared to recent proposals,¹⁵ narrower domain (bit) widths of about 150 nm (three times narrower) on average are obtained for $J = 2.0 \text{ TA/m}^2$ and $d = 0.4 \text{ ns}$, which gives an average greater bit density of $\sim 6 \text{ bits}/\mu\text{m}$ in the R strip. Note that due to the long-range dependence of the Oersted field, a standard bit-line architecture is not useful to nucleate subsequent DWs without perturbing the information already coded in the up or down domain between them (see details in Ref. 9). However, once the first DW is placed close to the junction with the R strip, our method does not require double bit lines, external multilayer attachments, magnetic fields, nor manipulating magnetic anisotropy to nucleate and shift subsequent DWs along the “recording strip” in a controlled manner. Note that these techniques may be only used once to generate the confined DW but are no longer required to sustain the process. Therefore, the proposed method significantly reduces the technological constraints for an iterative DW nucleation and the writing and transmitting of bits encoded in up or down domains.

See the [supplementary material](#) for (i) micromagnetic simulations of a conventional nucleation method for the initial DW, (ii) a detailed discussion on the reasons that may contribute to the reduction of J_C when the aperture angle (θ) increases, (iii) additional results for

narrower strips ($w = 10 \text{ nm}$), (iv) the analysis of the Field-Like (FL) torque, and (v) an investigation of the Joule heating effect on the proposed nucleation method.

This work was supported by Project No. SA114P20 from Junta de Castilla y León (JCyL) and, partially, by Project No. PID2020117024GB-C41 funded by Ministerio de Ciencia e Innovación, No. MAT2017-87072-C4-1-P from the Ministry of Economy, Spanish Government No. SA299P18 from JCyL, and MAGNEFI Grant agreement No. 860060 from the European Commission, European Union.

AUTHOR DECLARATIONS

Conflict of Interest

The authors have no conflicts to disclose.

Author Contributions

David Osuna Ruiz: Conceptualization (equal); Data curation (equal); Formal analysis (equal); Investigation (equal); Methodology (equal); Visualization (equal); Writing – original draft (equal); Writing – review & editing (equal). **Oscar Alejos:** Data curation (equal); Formal analysis (equal); Funding acquisition (lead); Investigation (equal); Methodology (equal); Project administration (lead); Resources (lead); Software (equal); Supervision (lead); Validation (supporting); Visualization (equal); Writing – review & editing (supporting). **Victor Raposo:** Data curation (equal); Formal analysis (equal); Funding acquisition (lead); Investigation (equal); Methodology (equal); Project administration (lead); Resources (equal); Software (lead); Supervision (lead); Validation (supporting); Visualization (equal); Writing – review & editing (supporting). **Eduardo Martínez:** Data curation (equal); Formal analysis (equal); Funding acquisition (equal); Investigation (equal); Methodology (equal); Project administration (equal); Resources (equal); Software (equal); Supervision (equal); Validation (equal); Visualization (equal); Writing – review & editing (equal).

DATA AVAILABILITY

The data that support the findings of this study are available from the corresponding author upon reasonable request.

REFERENCES

- ¹S. Parkin, M. Hayashi, and L. Thomas, *Science* **320**, 190 (2008).
- ²Z. Luo, A. Hrabec, T. Dao, G. Sala, S. Finizio, J. Feng, S. Mayr, J. Raabe, P. Gambardella, and L. Heyderman, *Nature* **579**, 214 (2020).
- ³P. P. J. Haazen, E. Mure, J. H. Franken, R. Lavrijsen, H. J. M. Swagten, and B. Koopmans, *Nat. Mater.* **12**(4), 299 (2013).
- ⁴S. Emori, U. Bauer, S.-M. Ahn, E. Martínez, and G. S. D. Beach, *Nat. Mater.* **12**(7), 611 (2013).
- ⁵E. Martínez, S. Emori, N. Perez, L. Torres, and G. S. D. Beach, *J. Appl. Phys.* **115**, 213909 (2014).
- ⁶J. Torrejon, E. Martinez, and M. Hayashi, *Nat. Commun.* **7**, 13533 (2016).
- ⁷K.-S. Ryu, L. Thomas, S.-H. Yang, and S. Parkin, *Nat. Nanotechnol.* **8**, 527 (2013).
- ⁸M. Benitez, A. Hrabec, A. Mihai, T. Moore, G. Burnell, D. McGrouther, C. Marrows, and S. Mcvitie, *Nat. Commun.* **6**, 8957 (2015).
- ⁹O. Alejos, V. Raposo, L. Sánchez-Tejerina, and E. Martinez, *Sci. Rep.* **7**, 11909 (2017).
- ¹⁰S. Zhang, W. Gan, J. Kwon, F. Luo, G. Lim, J. Wang, and W. S. Lew, *Sci. Rep.* **6**, 24804 (2016).

- ¹¹J. Nan, Y. Zhang, Z. Zhang, K. Zhang, Z. Zheng, G. Wang, X. Zhang, J.-O. Klein, D. Ravelosona, Y. Zhang, and W. Zhao, *IEEE Trans. Magn.* **55**, 9100204 (2019).
- ¹²Z. Luo, W. Liao, Y. Yang, C. Zhu, and Y. Wu, *Appl. Phys. Lett.* **111**, 162404 (2017).
- ¹³J. Franken, M. Hoeijmakers, R. Lavrijsen, J. Kohlhepp, H. Swagten, B. Koopmans, E. van Veldhoven, and D. Maas, *J. Appl. Phys.* **109**, 07D504 (2011).
- ¹⁴R. Lavrijsen, J. Franken, J. Kohlhepp, H. Swagten, and B. Koopmans, *Appl. Phys. Lett.* **96**, 222502 (2010).
- ¹⁵P. Dao, M. Müller, Z. Luo, M. Baumgartner, A. Hrabec, L. Heyderman, and P. Gambardella, *Nano Lett.* **19**, 5930 (2019).
- ¹⁶T. Phung, A. Pushp, L. Thomas, C. Rettner, S.-H. Yang, K.-S. Ryu, J. Baglin, B. Hughes, and S. Parkin, *Nano Lett.* **15**, 835 (2015).
- ¹⁷COMSOL AB, “COMSOL Multiphysics,” © v. 5.3a, www.comsol.com (COMSOL AB, Stockholm, Sweden, 2021).
- ¹⁸O. Alejos, V. Raposo, and E. Martínez, “Domain wall motion in magnetic nano-strips,” in *Materials Science and Technology* (American Cancer Society, 2020), pp. 1–49.
- ¹⁹A. Vansteenkiste, J. Leliaert, M. Dvornik, M. Helsen, F. Garcia-Sanchez, and B. Van Waeyenberge, *AIP Adv.* **4**, 107133 (2014).
- ²⁰E. Martinez, O. Alejos, M. Hernandez, V. Raposo, L. Sánchez-Tejerina, and S. Moretti, *Appl. Phys. Express* **9**, 063008 (2016).
- ²¹R. Real, V. Raposo, E. Martinez, and M. Hayashi, *Nano Lett.* **17**, 1814 (2017).